CONF-8510168--2

# DAMAGE ACCUMULATION IN CERAMICS DURING ION IMPLANTATION*

C. J. McHargue, G. C. Farlow, G. M. Begun, J. M. Williams, C. W. White, B. R. Appleton, P. S. Sklad, and P. Angelini

Oak Ridge National Laboratory
Oak Ridge, Tennessee 37831

CONF-8510168--2

DE86 001360

ABSTRACT

The damage structures of $\alpha$-$Al_2O_3$ and $\alpha$-SiC were examined as functions of ion implantation parameters using Rutherford backscattering-channeling, analytical electron microscopy, and Raman spectroscopy. Low temperatures or high fluences of cations favor formation of the amorphous state. At 300 K, mass of the bombarding species has only a small effect on residual damage, but certain ion species appear to stabilize the damage microstructure and increase the rate of approach to the amorphous state. The type of chemical bonding present in the host lattice is an important factor in determining the residual damage state.



## 1. Introduction

Ion implantation and ion beam mixing are being increasingly used to alter the near-surface of materials other than semiconductors. Recently there has been renewed interest in the study of the structure and properties of ceramics subjected to such treatments. Because of the non-equilibrium nature of such treatments and the complex nature of ceramic structures, progress in understanding the damage microstructures ha lagged behind that for metals and alloys.

*Research sponsored by the Division of Materials Sciences, U.S. Department of Energy, under contract DE-AC05-840R21400 with the Martin Marietta Energy Systems, Inc.

As a class of materials, ceramics (or insulators) have a wide variety of properties and structures. The chemical bonding ranges from ionic to covalent to near-metallic, and the atomic structure varies from crystalline to glassy. These materials are particularly sensitive to the chemical and electrical character of impurities or dopants. Damage due to bombarding ions may occur at different rates in the various sublattices due to differing masses or displacement energies for the different atomic species. Ion damage can occur as a result of ionization as well as displacement collisions; diffusion can have electrical and chemical driving forces; and phase changes can be introduced by damage or compositional changes.

In a review of defects and defect processes, Crawford concluded that the electronic properties of a few selected point defects in alkaline earth oxides, sapphire, and spinel are reasonably well understood. The residual radiation damage produced by irradiations that generate isolated point defects is likewise understood, but the production of the damage microstructure for high fluence neutron irradiation or heavy ion implantation damage is yet to be explained [1].

Studies of the optical absorption of $\alpha$-$Al_2O_3$ implanted with various gas ions and with aluminum ions have detected absorption bands at 4.8, 5.4, and 6.0 eV [2,3]. These absorption bands are characteristic of the $F^+$ and F centers, that is, oxygen vacancies containing one and two trapped electrons, respectively.

Using the Rutherford backscattering-channeling (RBS) technique, Drigo et al. [4] measured lattice disorder and lattice position for lead-implanted $\alpha$-$Al_2O_3$. They found saturation in the disorder for fluences greater than $10^{15}$ $Pb/cm^2$ and concluded that it indicated amorphization. At lower fluences,

about 70% of the implanted lead occupied aluminum lattice sites. They also concluded that aluminum and oxygen atoms were displaced in the stoichiometric ratio of 2:3.

Curves of lattice disorder (determined by RBS) introduced by 40 keV krypton ion bombardment of $\alpha$-$Al_2O_3$ had a sigmoidal form and reached a saturation value at a fluence of $1 \times 10^{16}$ ions/cm$^2$ [5]. Although the yield of the peak damage region for the aligned crystals never reached that of a random sample, Naguib and coworkers concluded that the saturation was indicative of the presence of amorphous regions. They also concluded that stoichiometry was preserved.

There has been great interest in the formation of the amorphous state in ceramics due to implantation damage [6–8]. Much of the discussion is based on studies of the evolution of implanted inert gases during subsequent annealing and the supposition that high rates indicated the presence of an amorphous phase or were due to a moving crystallization interface that swept the gas to the surface [9,10]. Reflection electron diffraction was also used by Matzke and Whitton [8] to characterize the surface of implanted $\alpha$-$Al_2O_3$. Diffuse halo patterns were observed for samples implanted with $2 \times 10^{16}$ ions/cm$^2$ of krypton or xenon (0.5 to 40 keV). The range of the inert gas ions in $\alpha$-$Al_2O_3$ was a few tens of nanometers.

Transmission electron micrographs of $\alpha$-$Al_2O_3$ implanted with inert gases (He, Ne, Ar) in the temperature range of 500 to 1250 K contained images of defect clusters and small dislocation loops for low fluences. At higher fluences, large numbers of pores or bubbles were present [11,12].

Investigations of the structure and electrical properties of implanted $\alpha$-SiC have been reported [13–19]. The amount of disorder, as measured by RBS, saturated at the value for a random sample for nitrogen and antimony [13–15].

About 50% of the implanted nitrogen occupied substitutional lattice sites at low fluences [13,15]. Evidence for C-C and Si-Si bonds and C-H, C-D, and Si-H bonds was obtained from Raman spectra taken from α-SiC specimens implanted with light gas ions to fluences reported to cause amorphization [18,19].

A number of criteria for predicting the amorphization of ceramics during irradiation have been proposed. Matzke and Whitton suggested that anisotropic non-cubic oxides are amorphized by low fluences of ions, whereas cubic materials remain crystalline to very high fluences [9]. Naguib and Kelly introduced a thermal spike model and a bond-type criterion [6]. The bond-type criterion predicts easy amorphization for materials whose Pauling ionicities are less than 0.6. The thermal spike model regards the disorder of the displacement cascade to be equivalent to a liquid. Considering the number of atomic jumps that occur as the temperature falls below the melting point, $T_m$, before reaching the crystallization temperature, $T_c$, gives the result that the material remains crystalline if $T_c/T_m < 0.27$ and becomes amorphous if $T_c/T_m > 0.27$. Such models do not allow for chemical interaction between implant species and cascade-produced defects. Kelly [20] also proposed a model for amorphization of oxides due to dispersed point defects in which randomization of an initial superlattice is caused by displacements and the low diffusivities of the atomic species are too low for long-range order to be re-established.

Parkin and Coulter have addressed the question of defect production in polyatomic materials where the mass and displacement energies of the various atom species may differ [21]. According to this model, details of defect production are most influenced by the initial PKA energy and the mass ratio of the atom types in the material.

This paper describes the damage accumulation in $\alpha$-$Al_2O_3$ and $\alpha$-SiC due to heavy ion implantation and is part of a continuing study at ORNL on the effects of ion implantation on the structure and properties of ceramics [22–25]. These materials have crystal structures that can be described by hexagonal axes but have very different bonding. The Pauling ionicity of $\alpha$-$Al_2O_3$ is 0.63 (intermediate ionic bonding) and that of $\alpha$-SiC is 0.12 (covalent bonding). A number of experimental techniques were used to determine the influence of implantation parameters (temperature, fluence, ion species) upon the damage structure of these two compounds.

## 2. Experimental Procedures

Single crystals of $\alpha$-$Al_2O_3$ (obtained from Crystal Systems, Inc., Salem, MA) with few impurities (<100 appm total) and low dislocation density ($10^3$–$10^4$/cm$^2$) were cut to within ±2° of <0001> or <$1\bar{2}10$>, polished, and annealed at 1400°C in air for 120 h to produce damage-free samples. Half of each sample was retained as virgin reference material and the remaining half was implanted with various ions at 77, 300, or 640 K. Current densities <2 $\mu$A/cm$^2$ were chosen to minimize beam heating to 100°C or less. The ion beam was incident at 7° or 3° from the crystal normal, and fluences ranging from $10^{15}$ to $10^{17}$/cm$^2$ were obtained at energies from 40 to 300 keV.

Both single crystals and polycrystalline samples of $\alpha$-SiC were used in the ORNL studies. Single crystal platelets in the (0001) orientation were produced by the Acheson furnace process at the Carborundum Company. They were predominantly of the 6H polytype. The polycrystalline material was sintered $\alpha$-SiC. Specimens were implanted with nitrogen (62 keV) or chromium (280 keV) at substrate temperatures of 300, 825, and 1025 K. The temperature of selected samples was measured by means of thermocouples mechanically clamped to the sample surface but not directly in the beam. Based on these measurements, it is estimated that the contribution of beam heating during low temperature implantations was ~100°C and significantly less during high temperature implantations.

Specimens were examined using Rutherford backscattering-ion channeling techniques (RBS-C) with 2.0 MeV $^4He^+$ to determine the depth profile of

the implanted species, the depth distribution of damage in the host lattice, and the lattice location of the impurity. One measure of damage or lattice disorder used in the following discussion is the minimum yield, $X_{min}$, determined for a particular sublattice at the depth of peak damage. The minimum yield is defined as the ratio of the backscattered yield from an aligned specimen to the yield from a randomly oriented specimen.

The data will be presented using displacements per atom (dpa) as the unit of fluence or dose in order to compare the effects from implanting ions of different masses and energies. The damage-energy density was calculated as a function of depth using the computer code E-DEP-1 [ref. 26] modified to incorporate the suggestions of Robinson and Oen [27]. These values of damage are approximately 20% higher than for the standard version. The number of displacements was calculated with the modified Kinchin-Pease equation [28]. For $\alpha$-$Al_2O_3$, the values of displacement energy determined by Pells and Phillips [29] were used, that is, $E_d^{Al}$ = 18 eV, $E_d^{O}$ = 72 eV. The value $E_d$ = 45 eV was used for both silicon and carbon in the case of SiC [30]. In both cases, one-half of the displaced atoms were considered to be cation species and one-half anion species, according to the treatment of Parkin and Coulter [21]. In the case of $\alpha$-$Al_2O_3$, the ratio of Al:O would be 40:60 instead of 50:50 if stoichiometry is maintained during damage production.

Specimens for TEM were prepared for both cross-section and plane viewing. Ion milling was used for thinning. Specimens were examined in a Philips EM400T/FEG equipped with 6585 STEM and EDAX 9100 x-ray EDS system. The probe size used was about 4 to 5 nm.

Raman spectra were recorded with a Ramanor HG-2S spectrophotometer (Jobin Yvon-Instruments SA). This instrument employs a double monochromator

with curved holographic gratings, cooled photoelectric detection, and pulse-counting electronics. A Nicolet 1170 signal averager was used to control the spectrometer and to accumulate the spectra from multiple scans. Spectra were excited with the 514.5 nm line of a Spectra-Physics model 164 argon-ion laser. A spike filter eliminated most of the plasma lines emitted by the laser. Light intensity focused on the sample varied from 0.2 to 0.5 W. The laser light, as observed with a long-focus microscope, was focused on the surface of the sample at 45° to the normal and the Raman scattering observed at 90° to the exciting laser light. The monochromator slits were parallel to the horizontal plane formed by the illuminating and scattered light. The polarization of the laser light was vertical.

## 3. Results and Discussion

### 3.1 Aluminum Oxide

All $\alpha$-$Al_2O_3$ samples of our study that were implanted at 300 K had a characteristic gray-brown color. Optical absorption measurements confirmed the presence of F and $F^+$ centers, representing electrons trapped at oxygen vacancies.

Figure 1 shows the backscattering spectra of 2 MeV $^4He^+$ ions from a crystal implanted with chromium (300 keV) to fluences of $1 \times 10^{16}/cm^2$ and $1 \times 10^{17}/cm^2$. After either fluence, the surface peaks from aluminum and oxygen are higher after implantation than in the virgin crystal, but the near-surface region is relatively damage free. The primary effect of increasing fluence was to extend the damage to greater depths with little increase in the magnitude of the damage level. Approximately 45% of the chromium occupied lattice sites on the aluminum sublattice at the $1 \times 10^{16}/cm^2$ fluence. Disorder in the oxygen sublattice was greater than in the aluminum sublattice

for all specimens examined. For the fluences shown in Fig. 1, the values were $x^{Al} = 0.66$ and $x^{O} = 0.88$.

Transmission electron micrographs (TEM) of these specimens showed a high concentration of defect clusters or small dislocation loops. Because of very high residual stresses, tilting experiments to deterine the character of these defects were unsuccessful [23].

The influence of fluence on disorder is shown in Fig. 2 for chromium implanted into $Al_2O_3$. Disorder in the aluminum sublattice, $x^{Al}$, remains constant at a value of 0.66 for the fluence range of 10.9 to 109 dpa for specimens implanted at 300 K. The saturation suggests that the defects are very mobile at these high damage levels such that defects are annihilated at the same rate as they are produced. This may be similar to the saturation noted by earlier investigators and interpreted as being due to the amorphous state [4,5]. Burnett and Page [31] report that $\alpha$-$Al_2O_3$ implanted with $6 \times 10^{17}$ Cr/cm$^2$ (300 keV) at 300 K had an amorphous surface layer, hence the curve in Fig. 2 must again increase to a value of unity. The fluence for their specimen corresponded to more than 600 dpa and the chromium-to-aluminum ratio was approximately unity.

The effect of substrate temperature on the resultant structure is shown in Figs. 2 and 3. The RBS spectra of Fig. 3 are from crystals implanted with $4 \times 10^{16}$ Cr/cm$^2$ (150 keV) at 77, 300, and 640 K. This fluence corresponds to 5.1 dpa. Disorder in the aluminum sublattice at the peak damage position is about the same for substrate temperatures of 300 and 640 K. The spectra show considerable recovery in the immediate surface layer for the higher substrate temperature. The degree of substitutionality of chromium was about the same for these temperatures (34% at 640 K, 29% at 300 K). The 77 K implant gave a scattering curve typical of an amorphous layer that extended to about 120 nm — well beyond the peak concentration of chromium. The amorphous nature of this

region was confirmed by TEM observations [24]. Figure 2 shows that the critical fluence for amorphization at 77 K (~3 dpa) is 200 times less than at 300 K (>600 dpa).

Implanting with foreign ions raises the question as whether chemical effects or displacement damage determines the phase(s) present after implantation. In order to remove possible chemical effects, specimens have been implanted with aluminum and oxygen ions in the stoichiometric ratio at 77 K ($4 \times 10^{16}$ Al/cm$^2$ at 90 keV, $6 \times 10^{16}$ O/cm$^2$ at 55 keV). The RBS spectra indicated an amorphous region that extended to a depth of about 150 nm [24]. Thus, damage alone can produce the amorphous state if recovery processes are suppressed; however, as will be shown, there may also be chemical effects.

Zirconium and zinc are the only cations to produce amorphous $\alpha$-$Al_2O_3$ at 300 K in our studies [32]. The RBS for zirconium (170 keV) gave a value of 0.75 for $\chi^{Al}$ after a fluence of $2 \times 10^{16}$/cm$^2$ (46 dpa) but a value of 1.0 after a fluence of $4 \times 10^{16}$/cm$^2$ (92 dpa). Figure 4 shows the TEM micrograph and selected area diffraction patterns for the latter sample. There is a buried amorphous layer that extends from 40 to 100 nm from the surface (zone B). Zones A and C show the damaged but crystalline material on either side of the amorphous layer. As the fluence was increased to higher values, the width of the amorphous region increased and eventually reached the surface. The RBS spectra showed that there was no tendency for zirconium to occupy substitutional lattice sites. Burnett and Page report amorphization for zirconium fluences a factor of 10 lower than for chromium [31].

In order to determine that the zirconium effect was not associated with changes in the cascade nature due to the higher mass, implants were made with niobium (having approximately one higher mass unit). The value of $\chi^{Al}$ for a

fluence of 90 dpa was 0.68 (compared to 1.0 for zirconium at dpa of 92). Thus, it appears that zirconium stabilizes the defects to prevent recovery processes or prevents the disordered regions within cascades from reordering. The data for Cr, Ti, Zr, and Nb are summarized in Fig. 5. In the range of fluences studied (to 110 dpa), the disorder in the aluminum sublattice is approximately the same for Cr, Ti, and Nb. The corresponding value for $x^0$ was about 0.9.

3.2 Silicon Carbide

The fluence required to amorphize covalently bonded α-SiC was more than 1000 times lower at 300 K than required for $Al_2O_3$. [Room temperature (300 K) is approximately 0.13 $T_m$ for $Al_2O_3$ and 0.11 $T_d$, decomposition temperature, for SiC.] Figure 6 shows the peak disorder in the silicon sublattice, $x^{Si}$, as a function of fluence, dpa. The energies of the nitrogen (62 keV) and Cr (280 keV) were chosen to give the ions approximately the same range in the target. There was a change in the slope of the curves indicating an acceleration in the rate of disordering after some initial period. These data also show a difference in disorder for the different ion species although the total defect production was the same.

Figure 7 shows the Raman spectra of a virgin α-SiC crystal and of similar crystals implanted with nitrogen (62 keV) to fluences of $2.7 \times 10^{15}$, $2.7 \times 10^{16}$, and $1.6 \times 10^{17}/cm^2$, corresponding to 0.54, 5.4, and 32 dpa, respectively. The two strong peaks at 789 and 967 $cm^{-1}$ are the transverse optical (TO) and longitudinal optical (LO) vibrations of the SiC crystal lattice. The auxiliary peaks at 150, 768, and 796 $cm^{-1}$ are characteristic of the 6H α-SiC polytype structure [33]. As SiC becomes disordered these peaks broaden until they vanish in amorphous samples.

In amorphous materials, all vibrational modes can contribute to the first-order Raman scattering [34], which results in a spectrum with broad peaks related to the density of states as determined by neutron scattering. In the case of SiC, the completely amorphous material shows very few spectral features.

With increasing nitrogen fluence, the peaks in the Raman spectra became weaker until all disappeared after 32 dpa irradiations indicating complete amorphization of the sample. The RBS spectra, on the other hand, showed that $x^{Si}$ (disorder in the silicon sublattice reached the value of 1.0 at a fluence of 0.2 dpa for 62 keV nitrogen ions (Fig. 6). The rising background of several of the spectra is due to traces of fluorescence attained during the implantation process.

Wright and co-workers [18,19] show broadened and weakened Raman peaks for the crystal vibrations of $\alpha$-SiC amorphized by $H^+$, $D^+$, and $He^+$ ion implantations. The RBS spectra showed that $x^{Si}$ (disorder in the silicon sublattice) reached the value of 1.0 at a fluence of 0.2 dpa for 62 keV nitrogen ions (Fig. 6). The penetration depth of the 514.5 nm exciting laser light for Raman spectra production varies greatly with the quality and color of the SiC crystals. Highly reflective samples produce weak spectra while clear samples give strong spectra. The virgin samples clearly gave light penetration to much grater depths than that of the expected ion penetration which is of the order of 0.2 μm. It is not clear whether the slow disappearance of the Raman spectral peaks with increasing fluence, as compared to the RBS data, was due to a spreading in depth of amorphization or to an increasing opacity of the surface layer of SiC. The latter explanation seems more likely.

There is no evidence in the spectra of Fig. 7 for the C-C or Si-Si bonds reported by Dolling and Cowley [35] for sputtered deposited amorphous SiC films. Thus, decomposition of the SiC by the bombarding ions is not indicated.

Broad bands centered at 1360 and 1585 $cm^{-1}$ (C-C bonds) or near 480 $cm^{-1}$ (Si-Si bonds) are reported for non-stoichiometric samples of SiC [36].

The Raman spectra for a virgin crystal of α-SiC and for one after implantation to 2.2 dpa with $2 \times 10^{15}$ Cr/$cm^2$ (260 keV) are shown in Fig. 8. The spectrum of the implanted sample contains no detectable peaks. Figure 6 shows that the amorphous (disordered) state as defined by RBS was reached at a fluence of 0.25 dpa. In our studies, the Raman peaks disappeared in the chromium-implanted samples at much lower fluences than for nitrogen-implanted samples, possibly indicating a more rapid increase in the opacity of the surface layer.

As in the case of α-$Al_2O_3$, raising the substrate temperature allows recovery processes to occur or bonds to reform and delays the onset of amorphization in α-SiC. Figure 9 shows the RBS spectra for samples implanted with nitrogen (62 keV, $8 \times 10^{16}/cm^2$) or chromium (260 keV, $1 \times 10^{16}/cm^2$) at 1023 K (750°C). The spectra show that neither specimen became amorphous. The values of $x^{Si}$ and dpa were 0.85 and 16.8, respectively, for the nitrogen implants and 0.6 and 9 dpa, respectively, for the chromium implants. These dpa levels are 45 to 100 times those that produced amorphous structures at 300 K.

## 4. Summary

The accumulation of disorder in the cation sublattice of α-$Al_2O_3$ and α-SiC, and the formation of an amorphous state during ion implantation have been measured as a function of important implantation parameters: fluence, substrate temperature, and ion species. Covalent bonded α-SiC reaches an amorphous condition at a fluence $10^{-3}$ that required for α-$Al_2O_3$ at approximately 0.1 $T_m$. Substrate temperature is particularly important for both

materials, since dynamic recovery processes determine the residual structure at higher temperatures. The rate of damage accumulation is faster for nitrogen than for chromium in $\alpha$-SiC. Similarly, zirconium produces the amorphous state in $\alpha$-$Al_2O_3$ at 300 K at a fluence about ten times less than does chromium.

## References


[1] J. H. Crawford, Jr., Nucl. Instr. and Meth. Phys. Res. B1 (1984) 159–165.

[2] G. W. Arnold, G. B. Krefft, and C. B. Norris, Appl. Phys. Lett. **25** (1974) 540-542.

[3] B. D. Evans, H. D. Hendricks, F. D. Bazzarre, and J. M. Bunch, Ion Implantation in Semiconductors, 1976, eds. F. Chernow, J. A. Borders, and D. K. Brice (Plenum Press, New York, 1976) pp. 265–274.

[4] A. V. Drigo, S. LoRusso, P. Mazzoldi, P. D. Goode, and N.E.W. Hartley, Rad. Eff. **33** (1977) 161–171.

[5] H. M. Naguib, J. F. Singleton, W. A. Grant, and G. Carter, J. Mat. Sci. 8 (1973) 1633–1640.

[6] H. M. Naguib and R. Kelly, Rad. Eff. 25 (1975) 1–12.

[7] R. Kelly, Nucl. Instr. and Meth. 182/183 (1981) 351–378.

[8] Hj. Matzke, Rad. Eff. **64** (1982) 3–33.

[9] Hj. Matzke and J. L. Whitton, Canadian J. Phys. **44** (1966) 995–1010.

[10] C. Jech and R. Kelly, J. Phys. Chem. Solids **30** (1969) 465–474.

[11] M. D. Rechtin, Rad. Eff. 42 (1979) 129–144.

[12] W. E. Lee, G. P. Pells, and M. L. Jenkins, J. Nucl. Mat. 122/123 (1984) 1393–1397.

[13] R. Hart, H. Dunlap, and O. Marsh, Rad. Eff. **9** (1971) 261–266.

[14] O. J. Marsh, Silicon Carbide—1973, eds. R. C. Marshall, J. W. Faust, Jr., and C. E. Ryan (University of South Carolina Press, Columbia, SC, 1973) pp. 471—485.

[15] A. B. Campbell, J. B. Mitchell, J. Shewchun, D. Thompson, and J. A. Davies, ibid. pp. 486—492.

[16] W. J. Choyke, L. Patrick, and P. J. Dean, Phys. Rev. B10 (1974) 2554—2560.

[17] D. A. Thompson, M. C. Chan, and A. B. Campbell, Canadian J. Phys. 54 (1976) 626—632.

[18] R. B. Wright, R. Varma, and D. Gruen, J. Nucl. Mat. 63 (1976) 415—421.

[19] R. B. Wright and D. Gruen, Rad. Eff. 33 (1977) 133—140.

[20] R. Kelly, Nucl. Instr. and Methods 182/183 (1981) 351—373.

[21] D. M. Parkin and C. A. Coulter, J. Nucl. Mat. 103/104 (1981) 1315—1318.

[22] H. Naramoto, C. W. White, J. M. Williams, C. J. McHargue, O. W. Holland, M. M. Abraham, and B. R. Appleton, J. Appl. Phys. 54 (1983) 683—698.

[23] C. J. McHargue and C. S. Yust, J. Am. Ceram. Soc. 67 (1984) 117—123.

[24] C. J. McHargue, G. C. Farlow, C. W. White, J. M. Williams, B. R. Appleton, and H. Naramoto, Mat. Sci. Eng. 69 (1985) 123—127.

[25] J. M. Williams, C. J. McHargue, and B. R. Appleton, Nucl. Instr. and Methods 209/210 (1983) 317—323.

[26] I. Manning and G. P. Mueller, Comp. Phys. Commun. 7 (1974) 85—94.

[27] M. T. Robinson and O. S. Oen, J. Nucl. Mat. 110 (1982) 147—149.

[28] M. J. Norgelt, M. T. Robinson, and I. M. Torrens, Nucl. Eng. Design 33 (1974) 50—56.

[29] C. P. Pells and D. C. Phillips, J. Nucl. Mat. 80 (1979) 215—222.

[30] F. W. Clinard, Jr., to be published in Radiation Effects in Crystals, eds. R. A. Johnson and A. N. Orlov (North-Holland, Amsterdam).

[31] P. J. Burnett and T. F. Page, J. Mat. Sci. 19 (1984) 3524–3545.

[32] G. C. Farlow, C. J. McHargue, C. W. White, and B. R. Appleton, to be published in Journal Materials Research.

[33] D. W. Feldman, J. H. Parker, Jr., W. J. Choyke, and L. Patrick, Phys. Rev. 170 (1968) 698–704.

[34] J. E. Smith, Jr., M. H. Brodsky, B. L. Crowder, and M. I. Nathan, Phys. Rev. Lett. 26 (1971) 642–646.

[35] G. Dolling and R. A. Cowley, Proc. Phys. Soc. London 88 (1966) 463–476.

[36] P. Krautwasser, G. M. Begun, and P. Angelini, J. Amer. Ceram. Soc. 66 (1983) 424–434.

## FIGURE CAPTIONS

Fig. 1. Backscattering spectra of 2 MeV $H^+$ from $^{52}Cr$ (300 keV, $10^{16}$ and $10^{17}/cm^2$) implanted $\alpha$-$Al_2O_3$ at 300 K.

Fig. 2. Disorder in the aluminum sublattice ($\chi^{Al}$) as a function of fluence (displacements per atom) for chromium implanted into $\alpha$-$Al_2O_3$ at 77 and 640 K.

Fig. 3. Backscattering spectra from $\alpha$-$Al_2O_3$ implanted with $4 \times 10^{16}$ $Cr/cm^2$ (5.1 dpa) at 77, 300, and 640 K.

Fig. 4. Cross section TEM micrograph and selected area diffraction patterns for $\alpha$-$Al_2O_3$ implanted with $4 \times 10^{16}$ $Zr/cm^2$ (170 keV, 92 dpa) at 300 K.

Fig. 5. Disorder in the aluminum sublattice ($\chi^{Al}$) as a function of fluence (dpa) for $\alpha$-$Al_2O_3$ implanted with Cr, Ti, Nb, and Zr at 300 K.

Fig. 6. Disorder in the silicon sublattice ($\chi^{Si}$) as a function of fluence (dpa) for $\alpha$-SiC implanted with nitrogen (62 keV) and chromium (280 keV) at 300 K.

Fig. 7. Raman spectra from $\alpha$-SiC implanted with nitrogen (62 keV) to 0.54, 5.4, and 32 dpa at 300 K.

Fig. 8. Raman spectra from $\alpha$-SiC implanted with chromium (280 keV) to 2.2 dpa at 300 K.

Fig. 9. Backscattering spectra from $\alpha$-SiC implanted with nitrogen (62 keV, $8 \times 10^{16}/cm^2$, 16.8 dpa) and chromium (280 keV, $1 \times 10^{16}/cm^2$, 9 dpa) at 1023 K.

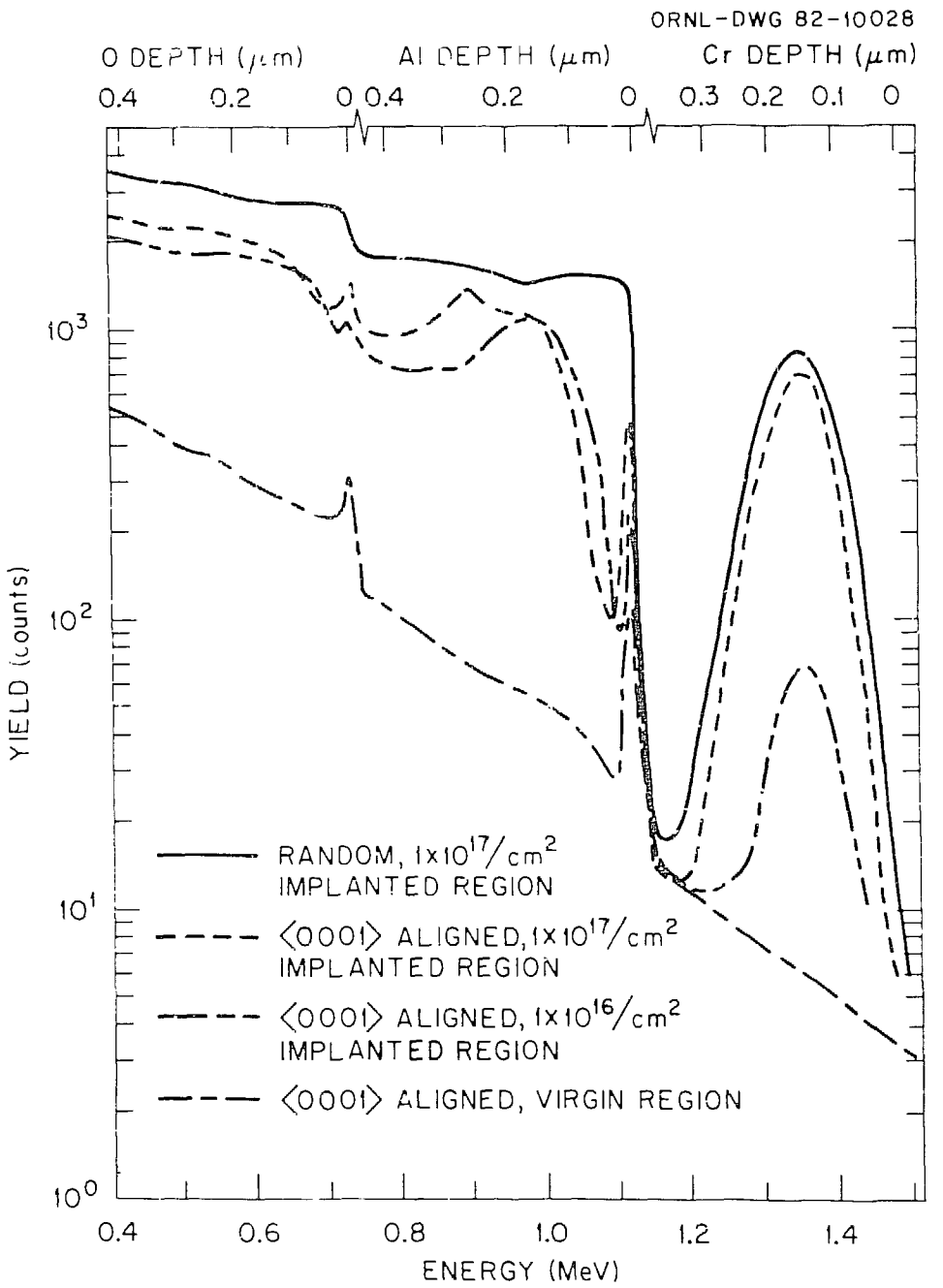


Damage Distributions For $^{52}Cr$ (300 keV) In $\alpha-Al_2O_3$

Fig. 1

ORNL-DWG 85-15411

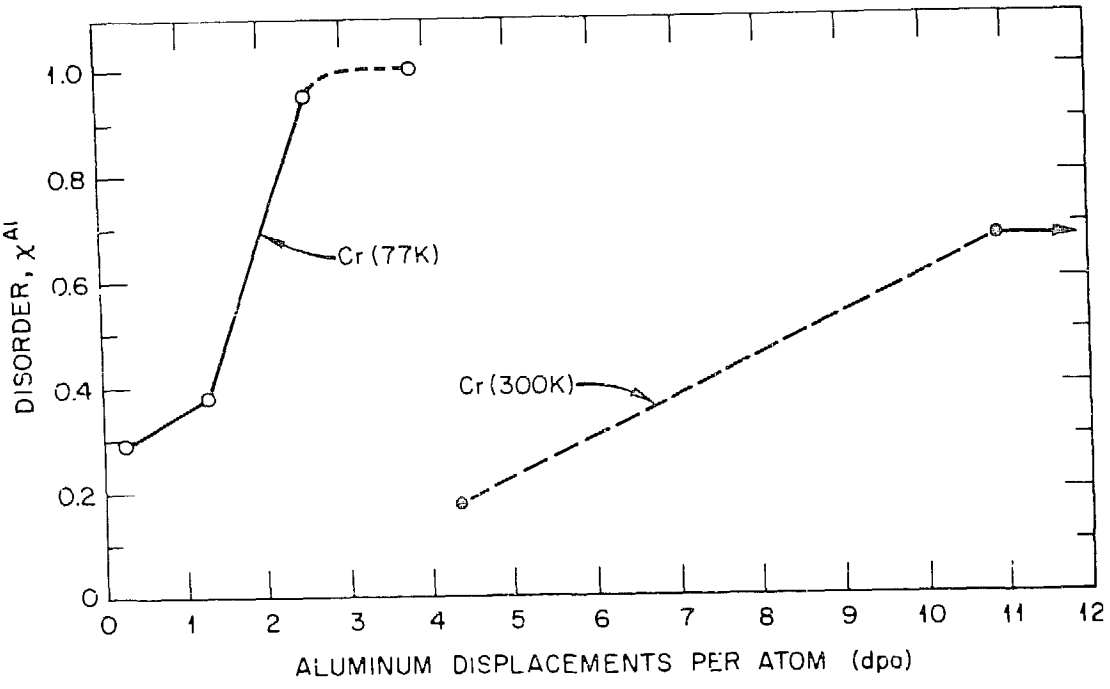


ORNL-DWG 83-14164

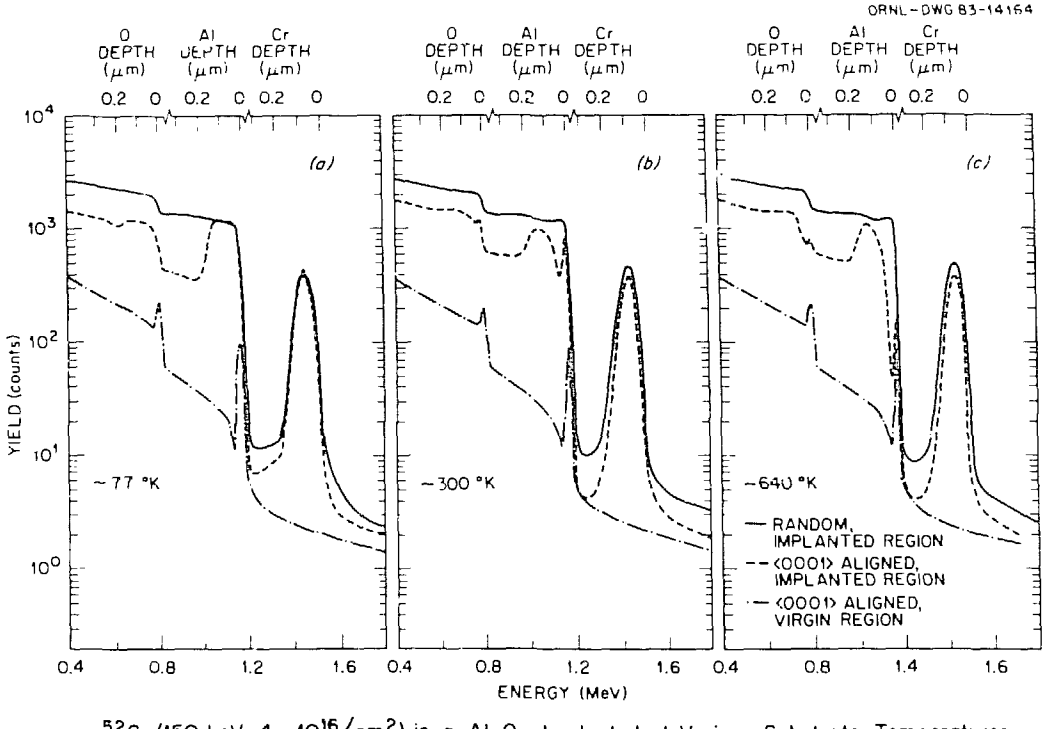


$^{52}Cr$ (150 keV, $4 \times 10^{16}/cm^2$) in $\alpha$-$Al_2O_3$ Implanted at Various Substrate Temperatures

ORNL-Photo 6470-83

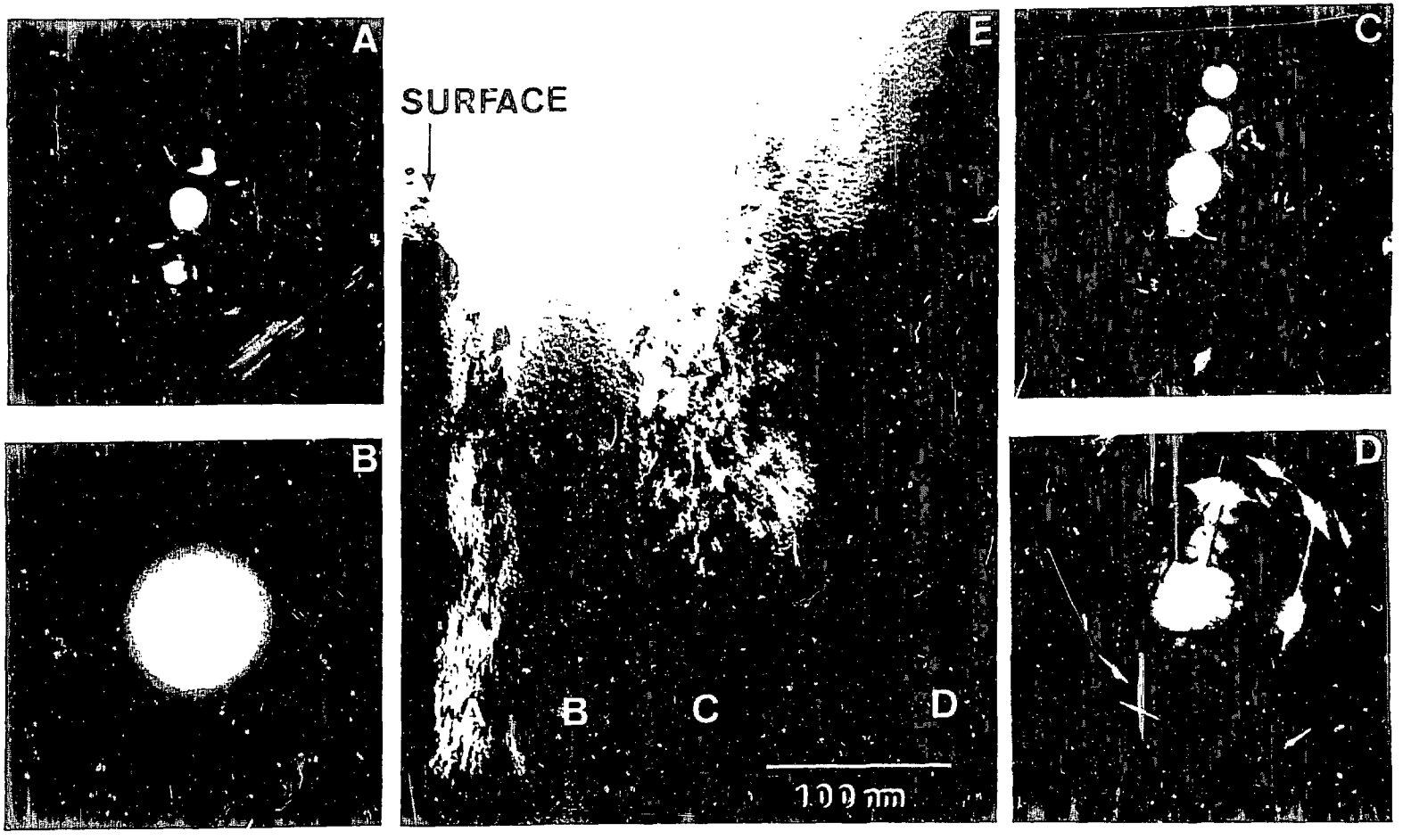


Fig. 5

ORNL-DWG 85-15412

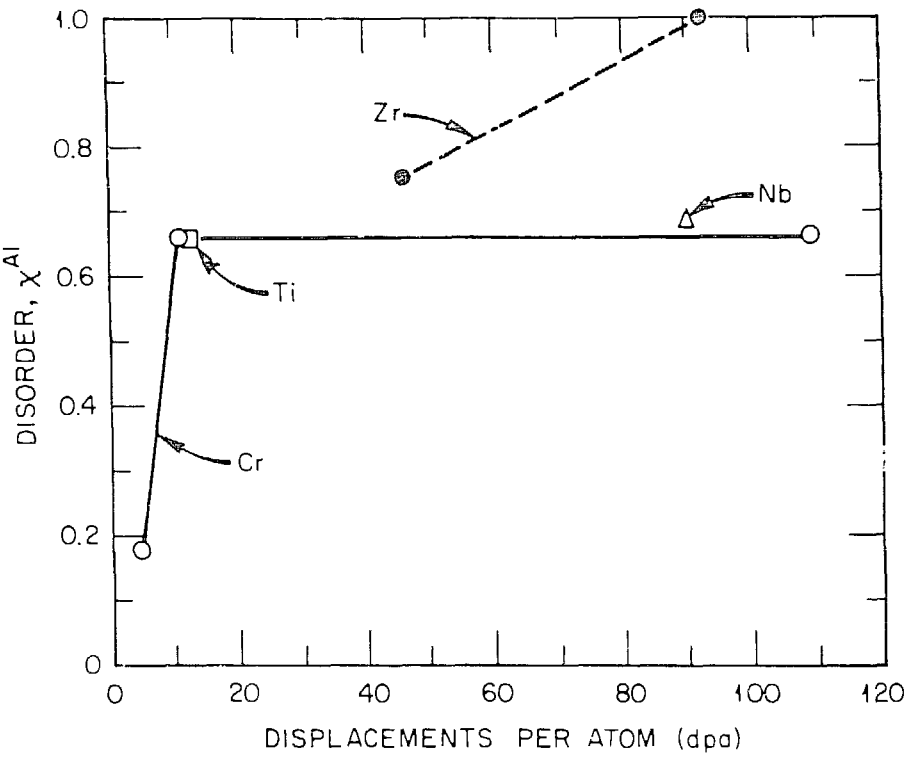


ORNL-DWG 85-15413

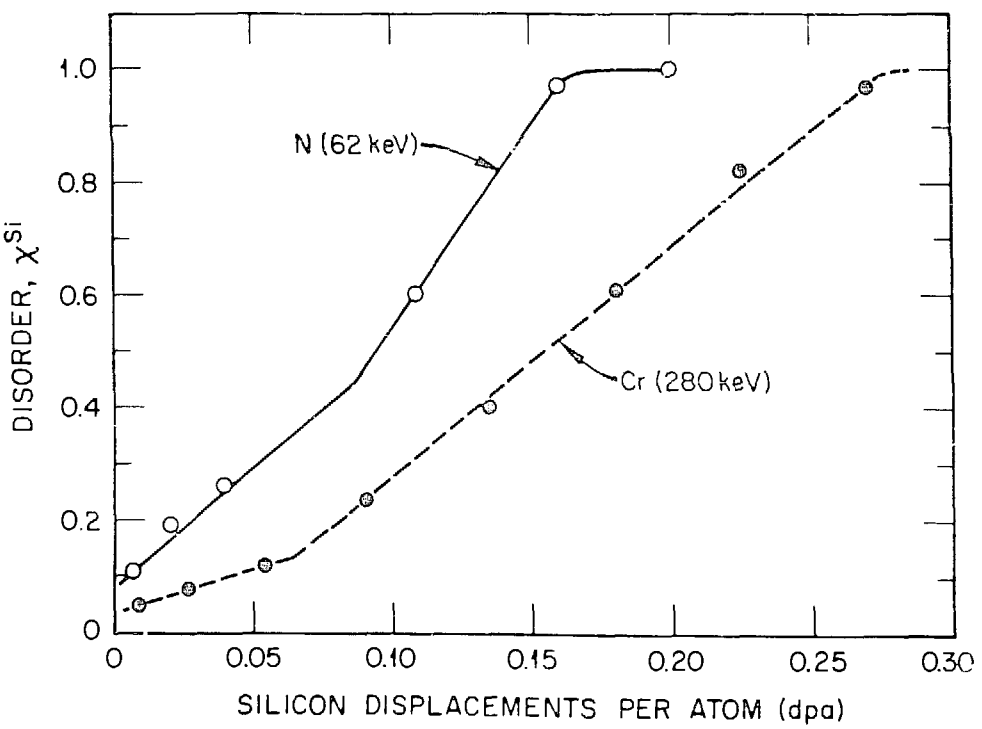

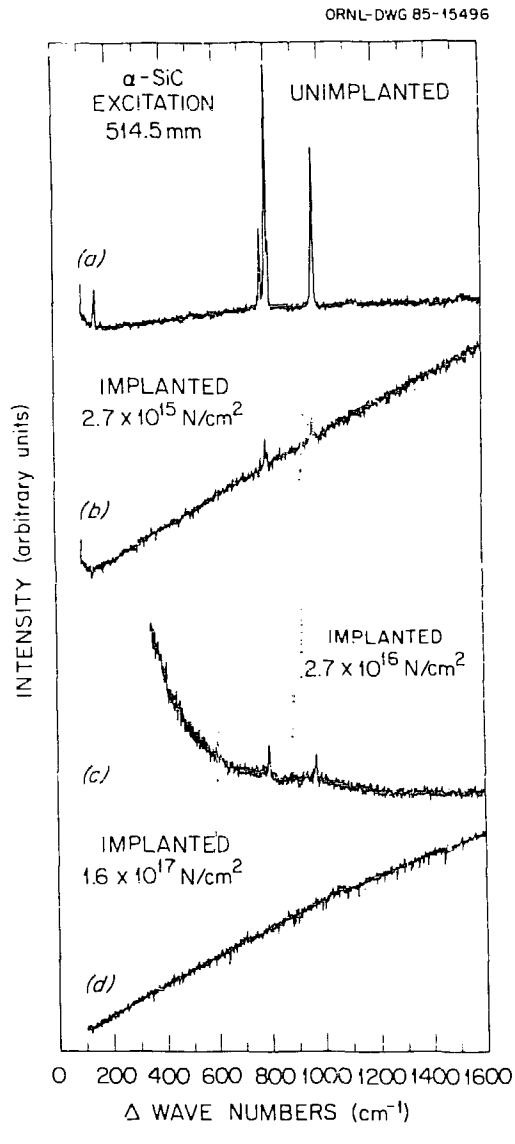
ORNL-DWG 85-15496
α-SiC
EXCITATION
514.5 mm
UNIMPLANTED
(a)
IMPLANTED
2.7 x 10^15 N/cm^2
(b)
IMPLANTED
2.7 x 10^16 N/cm^2
(c)
IMPLANTED
1.6 x 10^17 N/cm^2
(d)
INTENSITY (arbitrary units)
0 200 400 600 800 1000 1200 1400 1600
Δ WAVE NUMBERS (cm^-1)

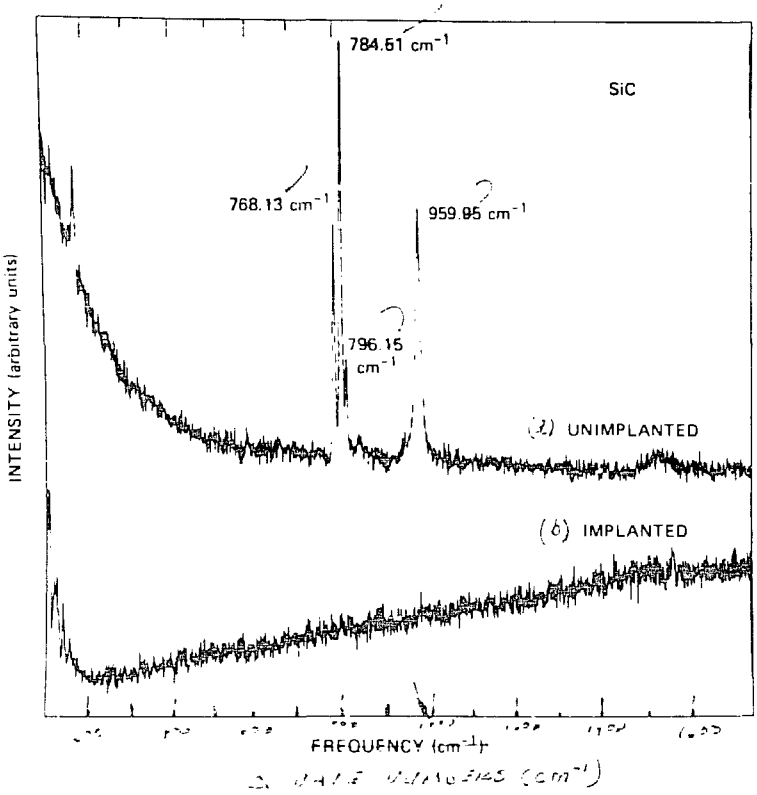
784.61 cm⁻¹
SiC
768.13 cm⁻¹
959.85 cm⁻¹
796.15 cm⁻¹
(a) UNIMPLANTED
(b) IMPLANTED
INTENSITY (arbitrary units)
FREQUENCY (cm⁻¹)

ORNL-DWG 85C-13233

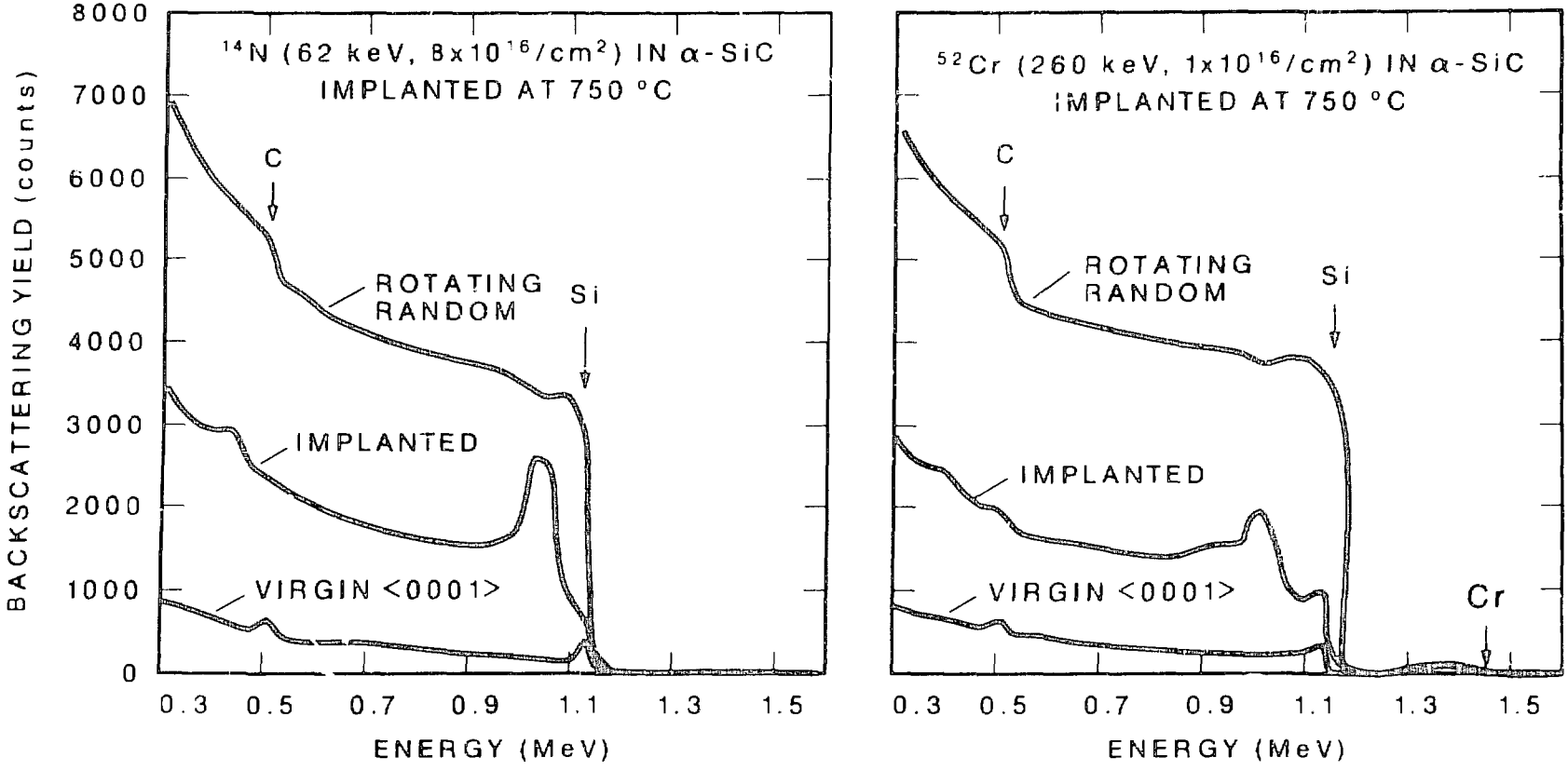


Fig. 2